Food Chemistry 370 (2022) 131376

Contents lists available at ScienceDirect

Food Chemistry

journal homepage: www.elsevier.com/locate/foodchem

Targeting mangiferin loaded N-succinyl chitosan-alginate grafted nanoparticles against atherosclerosis – A case study against diabetes mediated hyperlipidemia in rat

Ying Wang [a], Tanushree Karmakar [b], Nilanjan Ghosh [c], Souvik Basak [b,*], Nanda Gopal Sahoo [d,*]

[a] Ophthalmology and Otorhinolaryngology, Xi 'an No. 3 Hospital, Xi'an, Shaanxi 710018, China
[b] Dr. B.C. Roy College of Pharmacy & Allied Health Sciences, Durgapur, WB, India
[c] Department of Pharmaceutical Technology, Jadavpur University, Kolkata, West Bengal, India
[d] Department of Chemistry, Kumaun University, D.S.B. Campus, Nainital, Uttrakhand, India

ARTICLE INFO

Keyword:
N-succinylated chitosan
MGF
COSY
Diabetes
Cholesterol

ABSTRACT

Mangiferin (MGF), from *Mangifera indica* is well reported for its hypoglycemic activity and hypolipidemic activity. However, MGF suffers therapeutic limitation due to poor solubility causing disparaging bioavailability. Herein to address this problem, we have incorporated MGF in alginate grafted N-succinylated chitosan (NSC) nanomatrix. Characterization by molecular docking, FT-IR and 2D-NMR (COSY) has revealed that MGF could reinforce interaction with NSC. The —OH and —CH_2OH groups of MGF may set interactions with pyranosic —OH, —CH_2OH, —NH_2 (or —NH-succinyl and —COOH-succinyl) of NSC. The NSC-MGF nanoconjugate revealed a spherical particle geometry of 100 ~ 200 nm size. The encapsulated MGF showed 100% release *in vitro*. In vivo, NSC-MGF nanoconjugate revealed blood glucose lowering from 300 mg/dL to ~ 90 mg/dL as well as ~ 37% lowering of total plasma cholesterol. This is well comparative to the earlier reports which acknowledged only 1 ~ 36% lowering of plasma cholesterol with MGF. Furthermore, NSC-MGF lowered serum trigyceride to ~ 61%, while in earlier studies, only 10 ~ 40% serum triglycerides reduction was found with solitary MGF.

1. Introduction

Diabetes mellitus and its correlated complications have become a major global health concern that is affecting the worldwide population through its co-morbidities. According to International Diabetes Federation (IDF), approximately 463 million adults were diabetic in 2019; and the number of diabetic adults may rise to 700 million by 2045. Diabetes is a complex metabolic endocrine disorder, characterized by deficient insulin signaling, glucose metabolism, fat and protein metabolism leading to different macrovascular and microvascular complications (Ohiagu, Chikezie, & Chikezie, 2021). Apart from the vascular complications, several secondary complications such as diabetic neuropathy, retinopathy, nephropathy, cardiomyopathy, and foot diseases develop in long term diabetic patients (Alam et al., 2021; Papatheodorou, Banach, Bekiari, Rizzo, & Edmonds, 2018; Silva, Ferreira, & de Pinho, 2017). Hyperglycemia alters the hormonal and the enzymatic balance thus modulating normal physiological homeostasis leading to a disturbed metabolic state. The vicious role of lipotoxicity owing to lipid metabolism in adipose and other tissues worsens the diabetic complications by modulating several other inflammatory mediators and free radicals at the molecular level, thus triggering a negative downstream cascade of events (Katakami, 2018; la Sala et al., 2019; Poznyak et al., 2020). Risk factors like obesity further contribute to glucose and lipid accumulation resulting in glucotoxicity and lipotoxicity which are involved in development of life threatening cardiovascular, cerebrovascular and peripheral events (Di Pino & Defronzo, 2019). Insulin resistance can promote both atherogenesis and advanced plaque progression, and thus increases the risk for coronary artery disease (Di Pino & Defronzo, 2019; Stolar &

Abbreviations: AGEs, Advanced Glycation Endproducts; ALG, Alginate; BNT, Blank Nanaoparticle Treated group; COSY, Correlation Spectroscopy; CPCSEA, Committee for the Purpose of Control and Supervision of Experiments on Animals; DC, Diabetic control; DCM, Diabetic Cardiomyopathy; DLS, Dynamic Light Scattering; DMSO, Dimethyl Sulphoxide; FT-IR, Fourier Transformed Infrared Spectroscopy; IAEC, Institutional Animal Ethical Committee; JNK, c-Jun *N*-terminal kinase; MAPK, protein kinase; MGF, Mangiferin; MMFF94, Molecular Mechanics Force Field 94; MNT, MGF loaded Nanoparticle Treated group; MT, Free MGF Treatment group; NC, Normal control; NMR, Nuclear Magnetic Resonance Spectroscopy; NSC, *N*-Succinyl Chitosan; SC, Standard control; XRD, X Ray Diffraction.

* Corresponding authors.
E-mail addresses: souvik_basak1@yahoo.com (S. Basak), ngsahoo@yahoo.co.in (N. Gopal Sahoo).

https://doi.org/10.1016/j.foodchem.2021.131376
Received 8 July 2021; Received in revised form 5 October 2021; Accepted 6 October 2021
Available online 9 October 2021

Chilton, 2003). Presently, the mainstay of hyperglycemia management involves oral hypoglycemic drugs including biguanides (metformin and analogues), sulphonylureas (chlorpropamide, glibenclamide, glipizide, glimipride) α-glucosidase inhibitors (acarbose, miglitol), Peroxisome Proliferator Activated Receptor-γ (PPAR-γ) agonists (Rosiglitazone, Pioglitazone and others), Dipeptidyl peptidase-4 (DPP-4) inhibitors (Sitagliptin, Vildagliptin, Saxagliptin), sodium glucose cotransporter-2 (SGLT-2) inhibitors (canagliflozin, dapagliflozin, empagliflozin) and others (Choi et al., 2010; May & Schindler, 2016; Stein, Lamos, & Davis, 2013). However, the beneficial effects of these drugs are offset by prominent adverse effects such as hypoglycemia, nephrotoxicity, hepatotoxicity and impaired cardiac functioning (Kaur, Kumar, Parkash, & Prasad, 2019; Tsang, 2012). Thus, only a few of them are able to impede the disease progression without perturbing adverse effects (Luna & Feinglos, 2001). Therefore, there has been a demand seeking alternative therapies that may more importantly halt the disease progression along with fewer adverse effects.

In this search, attempt has been performed to nail out phytoconstituents that offer antidiabetic properties because these compounds generally offer lesser side effects than synthetic analogues (Gaikwad, Krishna Mohan, & Rani, 2014; Gupta, 2018; Singh, Kaur, Kishore, & Kumar Gupta, 2013). Mangiferin (MGF) is a C-glucosyl xanthone phytoconstituent isolated from mango (*Mangifera indica*). Chemically it is 1, 3, 6, 7–tetrahydroxyxanthone–*C*2–β–D–glucoside and holds bioactive potential in management of diabetes mellitus. It improves β-cell function and promotes insulin secretion to lower blood glucose level, in addition stabilizes adipokine formation which is formed post hyperglycemia in blood and finally downregulates adipose tissue formation (Aswal et al., 2020; Muruganandan, Srinivasan, Gupta, Gupta, & Lal, 2005; Sellamuthu, Arulselvan, Muniappan, Fakurazi, & Kandasamy, 2013). MGF inhibits metabolic enzymes such as mitogen activated protein kinase (MAPK), c-Jun *N*-terminal kinase (JNK) and regulates p38 molecular pathways to intercept diabetes-induced inflammatory, tumorogenic and cytokine pathways in blood which may be responsible for the aforementioned beneficial effects of MGF (Sellamuthu, Muniappan, Perumal, & Kandasamy, 2009). MGF has been found to ameliorate diabetic cardiomyopathy (DCM) by reducing levels of NF-κB and advanced glycation end products (AGEs) (Du, Liu, Lei, Xie, Wang, He, & Wang, 2018; Hou, Zheng, Fung, Deng, Chen, Liang, & Hu, 2013; Pal, Sinha, Sil, & Srinivasula, 2014; Sellamuthu et al., 2009). Moreover, MGF prevents hyperlipidemia by stimulating lipolysis and inhibiting lipogenesis. Thus, MGF could be an effective alternative to manage diabetes and associated hyperlipidemia with probabilistic lesser side effects owing to its phytochemical characteristics (Girón et al., 2009; Miura, Iwamoto, Kato, Ichiki, Kubo, Komatsu, & Tanigawa, 2001; Saleh, El-Maraghy, Reda, & Barakat, 2014; Zhang et al., 2019).

However, the major limiting factor in its therapeutic potential has been its very poor aqueous solubility and bioavailability. Low aqueous solubility (0.1 owing to 0.3 mg/mL) of MGF could be responsible for its low and variable oral bioavailability (about 1.5 to 5.0%). Many factors have been reported to contribute its low bioavailability, of which poor absorption post oral administration, high P-glycoprotein efflux, gastrointestinal metabolism and hepatic first-pass metabolism are noteworthy (Basheer & Kerem, 2015; Khurana et al., 2017; Ma, Chen, Sun, Tong, & Zhang, 2014). Multiple formulation strategies like cyclodextrin inclusion complex (Ferreira et al., 2013; Yang et al., 2013), phospholipid complex (Ma et al., 2014), and spray-dried encapsulation (de Souza et al., 2013) have already been reported in literature, but the results are far from satisfactory for clinical use. Thus evaluating the possible benefits that MGF can offer and the challenges present in its biopharmaceutical attributes, there is a need for development of more effective formulation strategies for MGF.

Nanotechnology often offered solution of improving drug solubility with choice of proper polymers as nanomaterial (Mukhopadhyay, Maity, Chakraborty, Rudra, Ghodadara, Solanki, & Kundu, 2016). To benefit from the potential offered by polymeric nanoformulations, we chose to prepare and characterize a novel polymeric nanoformulation using alginate (ALG) cross linked *N*-succinyl chitosan (NSC) as a potential nanocarrier for oral MGF delivery. Both NSC and ALG are pH sensitive, biodegradable, biocompatible, non-toxic, non-immunogenic, mucoadhesive and safe for oral treatment *in vivo* as described by (Mukhopadhyay et al., 2016, 2018). The use of chitosan may be limited by its poor solubility at neutral pH, which can be overcome by modifying chitosan into NSC, following methods described by (Bashir, Teo, Ramesh, Ramesh, & Khan, 2015; Kamoun, 2016). Presence of carboxylic acid groups confers excellent pH sensitivity exhibited by both NSC and ALG (Kato, Onishi, & Machida, 2004; Yan et al., 2006). The polymeric nanoparticles exhibit unique dual morphological structure having a core region and an outer shell. The active pharmaceutical moiety resides within the core region while the outer shell serves as the protective shield against lytic factors present in the gastro-intestinal tract (Mukhopadhyay et al., 2016). In the following study, NSC is first prepared using ring opening reaction of succinic anhydride in the presence of chitosan and acetic anhydride/glacial acetic acid. Characterization studies of the prepared samples involved particle size, encapsulation studies, *in vitro* MGF release kinetics, molecular docking, 2D NMR (COSY) analysis, fourier transform infrared spectroscopy (FT-IR), proton nuclear magnetic resonance (1H NMR), and X-ray diffraction study (XRD). In order to evaluate the therapeutic efficiency of the prepared delivery system, *in vivo* hypoglycemic effects, and effects on glucose and lipid homeostasis have been studied in streptozotocin (STZ) induced diabetic rat models.

2. Materials and methods

MGF, Chitosan powder [Medium molecular weight of 50,000–1,90,000 KDa; Degree of Deacetylation 75–85%], Streptozotocin, Nicotinamide and Succinic anhydride purchased from Sigma Aldrich (Aldrich, USA). Glacial acetic acid and Sodium alginate were supplied from institutional laboratory facility. All other chemicals and reagents were of analytical grade and were used without further modification

2.1. Animals

The study was conducted on the specific pathogen free Wistar rats of either sex weighing between 100 and 150 g (obtained from M/s Chakraborty Enterprise, Kolkata, India). The animals were first acclimatized under standard animal care guidelines which include room temperature of 24 ± 2 °C, relative humidity of 60 ± 5%, and 12/12 hr light dark cycle. Animals were fed with balanced diet (standard pellet food obtained from Hindustan Unilever, India) and water *ad libitum* for about 2 weeks prior to initiate the *in vivo* experiments. All the experiments were performed according to current guidelines for the care of the laboratory animals and the ethical guidelines for the investigation of experimental pain in conscious animals according to Committee for the Purpose of Control and Supervision of Experiments on Animals (CPCSEA) guidelines. All animal experiments in the present study were approved by Institutional Animal Ethical Committee (IAEC) of Dr B C Roy College of Pharmacy and AHS (Registration Number: BCRCP/IAEC/9/2019).

2.2. Molecular docking studies - evaluation of probabilistic binding dynamics between MGF and NSC

Molecular docking study was performed to evaluate the possible loading or binding interaction dynamics between MGF and NSC. The Glycosidic form of MGF (Supplementary Fig. S1A) and NSC (Fig. S1B) with seven repetitive subunits were drawn in ChemDraw Ultra (Perkin Elmer Inc., Waltham, Massachusetts, U.S.). Since NSC subunits are quite large, a chunk of the NSC with seven repetitive subunits was constructed to portray a trustable geometrical outfit of NSC participating in binding with MGF. In order to ensemble the interaction of the residual free —NH_2 terminals of NSC with MGF, a few —NH_2 groups were left untouched

during construction of the polymer. The 2D drawn structures were converted to 3D in Avogadro (Avogadro, molecular editor) and was energy minimized using Molecular Mechanics Force Field 94 (MMFF94) with steps per update 100 to obtain most favorable conformation. The molecules were opened in MGL Tools 1.5.2, added with polar hydrogens, equilibrated with Gasteiger and Kollman charges. The NSC was treated as macromolecule and was encaged in a grid box of dimension 48 Å × 50 Å × 40 Å having x, y and z centres at 2.836, 1.957 and 1.151. The docking was performed as per standard protocol and the results were analyzed in Discovery Studio Visualizer (Dassault Systemes BIOVIA, USA).

2.3. Preparation of MGF loaded NSC-alginate nanoparticles

NSC was prepared by ring-opening reaction using succinic anhydride in acetic acid media. 1 g of chitosan was first dissolved into 200 mL of 1 wt% glacial acetic acid solution and then transferred into a flask. 0.2 gm of Succinic anhydride was dissolved in 20 mL of acetone separately and was added into the flask by drop-wise for about 30 min at room temperature. The reaction mixture was then magnetically stirred at 40 for 4 to 6 hrs at 200 rpm. The reaction mixture was cooled to room temperature and precipitated in excess of acetone. The product was finally filtered to remove the excess of solvent present and allowed to get dried in a freeze dryer for about 24 hrs and used for further application and analysis. The chemical reaction of preparation of NSC has been outlaid in Fig. S2.

The nanoparticles were prepared by ionotropic gelation method using NSC, sodium alginate and calcium chloride as the cross-linker. NSC-alginate nanoparticles synthesis procedure was first optimized using varying concentration of the both. The optimum ratios of NSC and alginate for development of the conjugate assembly was established based upon several preliminary studies. Varying amounts of the compounds were incorporated together to investigate the effect of initial concentration to the consistency of the product so formed.

In a typical procedure, about 10 mL of 20 mg/mL NSC solution was prepared by magnetic stirring for about 30 mins following addition of 10 mL of 2 mg/mL sodium alginate solution drop wise and 1 mL of 10 mg/mL concentration calcium chloride solution was ultimately added to the resulting mixture and stirred occasionally for about 2 hrs to enhance the crosslinking of NSC molecules and alginate residues with the help of ionic cross linker. Loading of MGF into the system was made by dissolving the drug separately in ethanol at a concentration of 1 mg/mL following addition to NSC solution. The mixture was then sonicated in an Ultra sonic bath sonicator (LeelaSonic-50, 1.5 L) for about 30 mins and was kept overnight undisturbed to allow the formation of maximum conjugates. The product was then centrifuged at 4 °C at 10,000*g* for about 5–6 mins and was freeze-dried for further analysis. The NSC-Alginate crosslinked nanoparticle has been indicated as NSC nanoparticle during the entire study.

2.4. Characterization of N-succinyl-chitosan

.

2.5. FTIR analysis

Detection and analysis of modified as well as native chitosan were carried out by Fourier Transform Infrared Spectroscopy (FTIR). Samples were developed in form of KBr pellets and their individual spectra were recorded between 4000 and 400 cm^{-1} at room temperature on a Perkin Elmer Spectrum one equipment to examine the extent of chemical interactions of chitosan and succinic anhydride and hence its modification. FTIR spectra of succinic anhydride and sodium alginate were also performed to determine the nanoparticle characterization process.

2.6. $_1H^1$ NMR analysis

The $_1H^1$ NMR analysis of semisynthetic chitosan was performed in JEOL Nuclear Magnetic Resonance Spectroscopy instrument (JEOL Inc, MA, USA) using delta NMR software at 400 MHz using Tetra Methyl Silane (TMS) as reference. The compound was dissolved in DMSO-d_6 under inert atmosphere and the resonance spectra was recorded with 128 scan using delta NMR software with standard noise to signal enhancement protocol.

2.7. Determination of degree of substitution

The degree of substitution of succinyl chitosan was measured by potentiometric titration method. 0.1 g of succinyl chitosan was dissolved in 20 mL of distilled water and then the pH of the solution was adjusted to 2 by addition of 0.1 N hydrochloric acid solution. Then the resulting solution was titrated with 0.1 M sodium hydroxide solution and the corresponding pH values were noted with the help of a laboratory pH meter. The volume of the aqueous sodium hydroxide was determined, following which the degree of substitution was calculated as demonstrated by Mukhopadhyay et al., 2014:

$$Degree\ of\ Substitution = \frac{161A}{Mass\ of\ succinyl\ chitosan - 84A}$$

where A is the product of the volume of NaOH and molarity of NaOH used in the reaction system. 161 and 84 are the molecular weights of glucosamine and succinyl groups respectively.

2.8. Nanoparticles Characterization

2.8.1. FTIR analysis

FTIR analyses were performed for MGF loaded nanoparticles to detect the presence of individual drugs in the bipolymeric matrix system. The samples were analyzed using a Perkin-Elmer FT-IR spectrophotometer. Aliquots of samples were mixed with KBr, converted into pellets and hence examined. Each individual spectra of MGF loaded samples was recorded by scanning in between 400 and 4000 cm^{-1} and compared with that of spectrum of blank polymer matrix to determine the presence of the drugs in relevance to the individual FTIR spectra of MGF.

2.8.2. 2D NMR (COSY) analysis

The 2D NMR analysis (Correlation spectroscopy or COSY) was performed in JEOL NMR as described earlier with overnight scanning (total scan 32768) under standard conditions as described earlier. The X and Y domains were plotted with $_1H^1$ NMR signals and the proton-proton interaction was detected with relaxation delay 1.5 (s). The interaction dynamics were subsequently plotted as 2D contours in the XY plane.

2.8.3. Particle size and zeta potential analysis

The average particle size and zeta potential of the nanoparticles was determined using zeta sizer nano series (Malvern Panalytical, UK). The measurement was carried with ultra-pure water using zeta cells with general protocol at 25 °C. The mean zeta potential was determined using phase analysis light scattering technique.

2.8.4. Drug loading capacity, encapsulation efficiency

The amount of MGF encapsulated within the system was determined by measuring absorbance of the supernatant at 320 nm for MGF using UV–Vis spectrophotometry (Shimadzu UV-1700). The drug was first loaded into the system as described in 2.2 and then was centrifuged at 10,000*g*. The supernatant was collected, a definite volume of the same was spiked with methanol and subjected to spectrophotometric analysis at 320 nm. The concentration of MGF was determined using standard plot and the percentage of encapsulation efficiency of the polymeric system were calculated by the following relationship:

$$\text{Encapsulation Efficiency} = \frac{\text{Total drug in the formulation} - - \textit{Free}\text{Drug in the supernatant}}{\text{Total drug in the formulation}} \times 100$$

2.8.5. X-Ray diffraction studies

The powder XRD patterns of pure NSC, MGF and the nano-conjugate (NSC-MGF) were recorded by scanning with Goniometer = PW3050/60 (Theta/Theta) with filter Cu radiation over the interval 5–79°/2θ. A voltage of 40 kV, current 30 mA, filter Cu and scanning speed 1° / min was maintained throughout the operation.

2.8.6. In vitro drug release study

In vitro drug release study of MGF loaded nanoparticles were carried out in phosphate buffer saline (PBS) of pH 7.4. A 10 mg/mL suspension of the formulation was prepared in PBS medium. About 5 mL of the resuspended formulation was introduced into 200 mL of PBS with stirring at 100 rpm; the release studies being carried out at 37 °C. Sampling was performed at predetermined time intervals and the release media was replaced with fresh buffer solution to maintain the sink condition throughout the system. For each sample drawn, the absorbance values were noted at 320 nm for MGF formulation by diluting a suitable aliquot in methanol. Calibration curves were plotted for concentration-absorbance values and to calculate the amount of drug released from the formulations at different time intervals. The rate of release was calculated using the following equation:

Rate of Release [%] = (Released Drug/ Total Drug in the formulation) *100

2.8.7. Statistical analysis

The statistical analysis was performed using Kinet DS software (23) and Microsoft Excel (Microsoft Corporation, USA). The percent dissolution efficiency (% DE) for each sample was calculated as the percent ratio of area under the dissolution curve up to the time *t*, to that of the area of the rectangle described by 100 % dissolution at the same time (Hossain, Alam, & Paul, 2013; Simionato, Petrone, Baldut, Bonafede, & Segall, 2018) as follows:

$$\%DE = \left(\frac{\int_0^t y.dt}{y_{100}.t}\right)100 \quad (1)$$

Mean dissolution time (MDT) was calculated by the following expression (25):

$$MDT = \frac{\sum_{i=1}^{n} t_{mid}\Delta M}{\sum_{i=1}^{n}\Delta M} \quad (2)$$

In this mathematical expression for the calculation of MDT, i is the dissolution sample number, n is the number of dissolution times, t_{mid} is time at the midpoint between times $t_i$and t_{i-1}, and ΔM is the amount of drug dissolved between times $t_i$and t_{i-1}.

The difference factor (f_1) (Hossain et al., 2013)is given by:

$f_1 = \{[\sum_{i=1}^{n}|Ri - Ti|]/[\sum_{i=1}^{n}Ri]\} \times 100$

The similarity factor (f_2) [26] is given by:

$$f_2 = 50 \times log\left\{\left[1 + (1/n)\sum_{i=1}^{n}|R_i - T_i|^2\right]^{-0.5} \times 100\right\} \quad (3)$$

where i is the dissolution sample number, n is the number of dissolution times, R_i and $T_i$are the amount dissolved of the reference and the test drug sample at each time point i, respectively. It is 100 when the test and reference profiles are identical and approaches to 0 as the dissimilarity increases.

2.8.8. In vivo pharmacological response of the nanoparticles

Rats were subjected to hyperglycemia by intrapretonial (i.p) injection of freshly prepared streptozotocin (STZ) (dissolved in 0.1 M citrate buffer, pH 4.5) as a single dose (60 mg/kg body weight) in a volume of 1 mL/kg body weight. In order to prevent the STZ administered animals from going into hypoglycemic shock, 5% glucose solution was given *ad libitum*, for about 2–3 days along with standard pellet diet. The animals were monitored for a period of 14 days and their blood glucose levels were measured. Rats with stable fasting blood glucose levels (FBG) > 250 mg/dL were considered as stable hyperglycemic and were included in the study.

Random allocation of animals was done in the following six groups, with each containing 6 animals (n = 6);

Group 1; NC – Normal control

Group 2; DC – Diabetic control (STZ only)

Group 3; SC- Standard control; STZ induced diabetic rats treated with Glipizide (5 mg/kg b.w) orally for 28 days

Group 4; MT – Free MGF treatment group; STZ induced diabetic rats treated with free MGF (10 mg/kg b.w) orally for 28 days.

Group 5; BNT – Blank control group; STZ induced diabetic rats treated with blank nanoparticles orally for 28 days.

Group 6; MNT – nanoparticles loaded with MGF treatment group; STZ induced diabetic rats treated with MGF loaded core—shell nanoparticles (10 mg/kg b.w of MGF) orally for 28 days.

2.8.9. FBG and glucose tolerance test (GTT)

Blood glucose was monitored once a week throughout the experimental period. Blood sampling from the tail vein was collected before the first meal of the day to determine the FBG levels. The blood glucose levels were estimated using a glucometer (Accucheck) in blood samples collected from the lateral tail vein.

At the 4th week of the study, the experimental rats were subjected to an oral glucose tolerance test (OGTT). Blood samples were collected from the cut tails after fasting for 12 h (0th time), following which they were administered glucose solution by oral gavage (2 g/kg) and blood samples were again collected after 30, 60, 90 and 120 min. Blood glucose levels were estimated using an Accucheck glucometer. After 28 days of oral dosing, blood samples were collected from the retro-orbital plexus of overnight fasted rats of each group with mild general anesthesia and final blood glucose levels were determined.

2.8.10. Evaluation of serum lipid lowering activity-estimation of markers of atherosclerosis

Serum was separated from collected blood after 28 days and used for estimating the serum lipid profile such as total cholesterol (TC), triglyceride (TG), high-density lipoprotein (HDL) and cholesterol which are also the lipid markers for atherosclerosis. The above mentioned serum lipid parameters were estimated using diagnostic kits (Span Diagnostics Ltd, India). Comparative analysis was performed between untreated diabetic control and various treated groups as mentioned above and finally NSC-MGF contribution to such pharmacodynamic response is evaluated.

2.8.11. Statistical analysis

The results are expressed as mean ± SEM. Analysis of results was performed by one-way ANOVA followed by Tukey's test. Values of $p < 0.05$ were considered to be statistically significant.

3. Results and discussion

3.1. Chemical reaction and FTIR analysis of grafted NSC

The nano-conjugate was formed by incorporation of MGF (Fig. S1A) within shell like matrix of NSC (Fig. S1B). Preparation of NSC is basically a chemical cross linking reaction between chitosan and succinic anhydride in presence of acetic anhydride as catalyst.

The cross linking reaction between chitosan and succinic anhydride is basically guided by acetic acid which converts chitosan into chitosyl acetate and makes it water soluble. This step favors association of chitosan and succinic anhydride which is water soluble. Next, succinic anhydride coverts to an electrophile by ring opening reaction by acetic acid and attacks electron rich —NH_2 terminal of chitosan. Subsequently it forms NSC following a condensation reaction between the electrophile and electron donor (Fig. S2).

Analysis of FTIR spectral data represents an important characteristics in determining the extent of modification of native chitosan into succinyl chitosan by interaction with succinic anhydride in acetic acid medium. Fig. 1 depicts FTIR spectra of Chitosan, Succinic anhydride and Succinyl chitosan respectively. Fig. 1A- FTIR spectrum of native chitosan shows —NH and —OH stretching vibrations at 3435 cm^{-1}. The weak band at 2922 cm-1 may be due to the presence of —CH— stretching in chitosan molecule. The spectral data also shows distinctive vibration bands appearing at 1651 cm^{-1}, 1383 cm^{-1} depict 1°-NH_2 bend (free) and —CH_2 rock of solitary ungrafted chitosan respectively. The spectral data also shows distinctive vibration bands appearing at 1651 cm^{-1}, 1383 cm^{-1} depicts amide carbonyl stretch. The absorption band at 1154 cm^{-1} represents asymmetric stretching of C—O—C and the band at 1092 cm^{-1} corresponds to C—O stretching presenting characteristics of the saccharine backbone of chitosan. Fig. 1B-FTIR spectrum of succinic anhydride show characteristic grouping bands at 1862 cm^{-1} and 1785

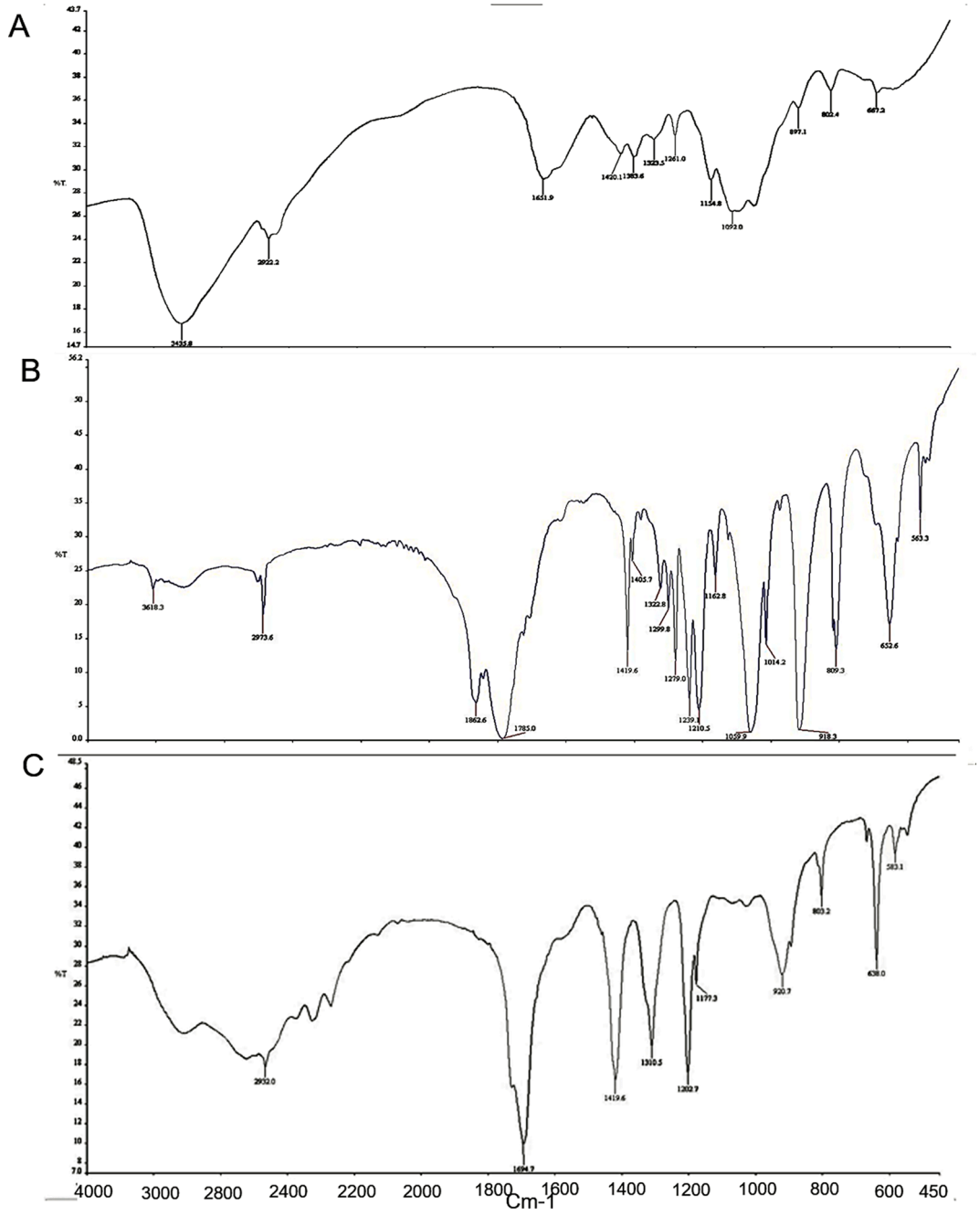

Fig 1. FT-IR Spectra of A. Chitosan B. Succinic anhydride C. Succinylated Chitosan.

cm^{-1} due to the presence of C═O stretching. Also, bands appearing at 1419 cm^{-1} and 1405 cm^{-1} correspond to CH_2 groups present in succinic anhydride. FTIR analysis of N –succinyl chitosan (Fig. 1C) shows the presence weak band at 2932 cm^{-1} representing the presence of —CH— stretching similar to chitosan. The absorption band at 1694 cm^{-1} and 1310 cm^{-1} also indicate the presence of amide carbonyl groups in the molecule. Interestingly, the 1651 cm^{-1} band in ungrafted chitosan has been totally abolished in grafted polymer (Fig. 1C) eliciting the participation of these —NH_2 terminals in cross-linking and thus converting to 2°-NH–.Furthermore, the strong carbonyl peaks at 1862 cm^{-1} and 1785 cm^{-1} in succinic anhydride have been significantly shifted to 1694 cm^{-1} in grafted chitosan suggesting the ring-opening of the same and forming the anticipated —NH—C═O— bond of NSC. The reduced bond energy of —*N*—C═O— in the final polymer compared to that of —O—C═O in succinic anhydride may be the cause of such a downfield shift of the associated band. The band appearing at 1419 cm^{-1} is similar to that of succinic anhydride due to the presence of CH_2 groups. The bands at 1202 cm^{-1}, 1177 cm^{-1} represent the saccharide backbone of the native chitosan molecule. Thus, the spectral data indicate succinyl modification of chitosan at the *N*-position and hence the subsequent formation of —NH—CO— groups.

3.2. $_1H^1$ NMR analysis of grafted chitosan (NSC)

The $_1H^1$ NMR spectra of NSCshows the following characteristics (Fig. 2):

$_1H^1$ NMR spectrum of NSC (400 MHz, DMSO-d_6, ppm) revealed that peaks corresponding to 2.12 ppm, 2.38 ppm and 2.54 ppm correspond to (-NH-CO-CH_3), (-NH-CO-CH_2) and (-CH_2-COO) protons in NCS. Peak at 2.70 ppm corresponds to H-2 of glucosamine.Peaks corresponding to 3.25, 3.68 and 3.86 ppm suggest glycosidic protons of glucosamine. Peaks at 5.47 ppm and 6.19 ppm correspond to β-CH of glycosidic carbon –CH-O-CH–, peak at 8.01 ppm denotes —NH proton of *N*-succinyl side chain of NSC. Furthermore, peak at 12.38 ppm correspond to —COOH proton of succinyl side chain.

3.3. Degree of substitution of NSC

Potentiometric titration was used to determine the degree of substitution of NSC. The degree of substitution was found to be 0.76 (76%) for a reaction system in which chitosan and succinic anhydride is of 1:2.

3.4. Molecular docking study of MGF and NSC

The molecular docking study revealed that MGF may successfully bind with NSC predominantly by hydrogen bonding interactions (Fig. S3). From tricyclic structure of MGF, the —C═O and proximal —OH groups participates in hydrogen bonding. Moreover, the oxygen bonds with polar —H from NSC —OH and side chain —NH of either free —NH_2 or succinylated —NH. Another interesting fact was observed that —NH of either free —NH_2 or succinylated —NH forms intramolecular hydrogen bonding with —COOH groups inside NSC molecule. In addition, carbonyl

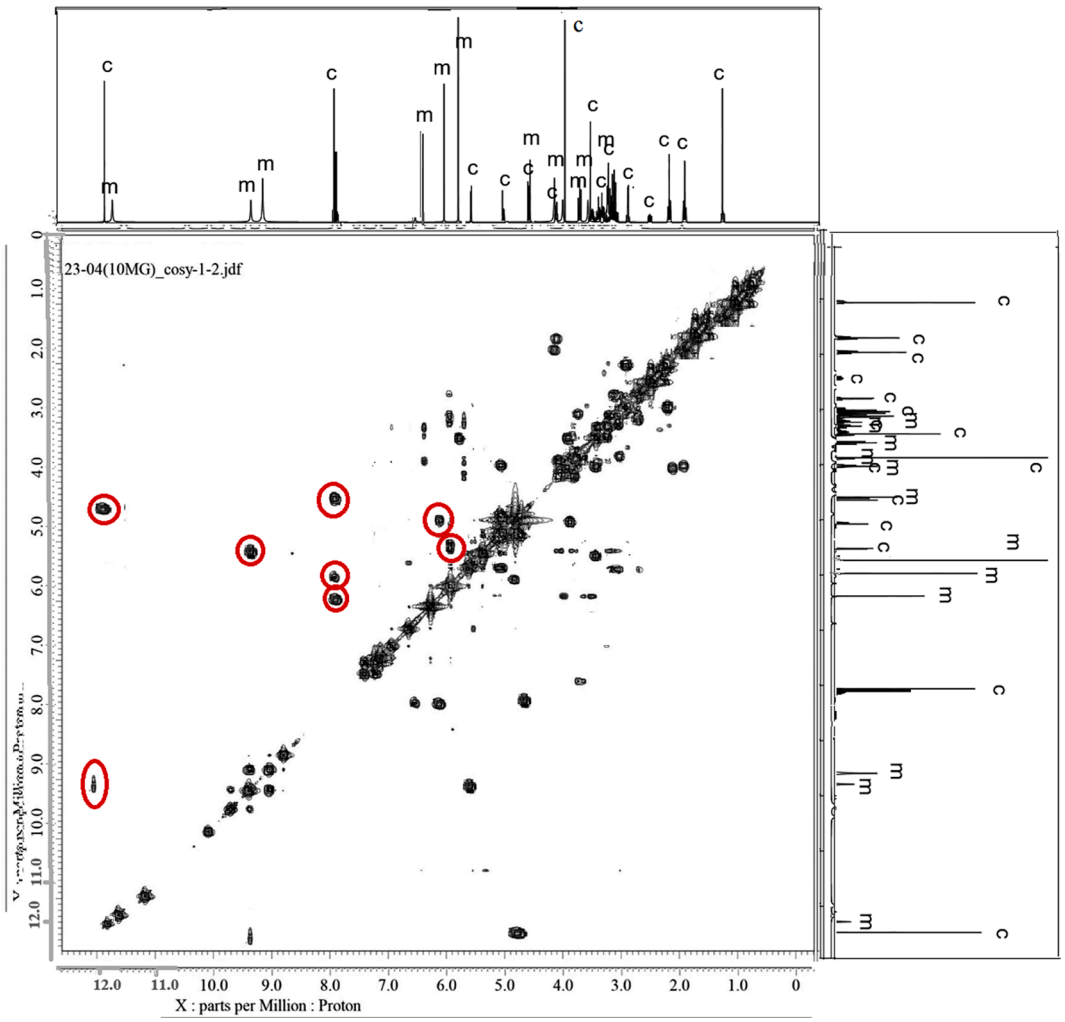

Fig 2. 2D NMR (COSY) spectra of MGF loaded NSC-alginate formulation. c-denotes proton peaks for NSC and m-depicts proton peaks for MGF.

oxygen of one succinyl side chain forms hydrogen bonding with another adjacent —NH depicting the importance of succinylation in forming stable formulation as well as the structure of the complex.

3.5. Encapsulation efficiency of MGF within NSC-alginate polymer based formulation

The formulation was prepared by ionic gelation technique with NSC and sodium alginate at a ratio of 10:1 and using calcium chloride as the cross linker. Spectra obtained for both of MGF nanoparticle formulation also confirms the presence of absorption bands of characteristics functional groups at 320 nm respectively. The encapsulation efficiencies were found to be 88.81 ± 0.56 % for MGF loaded formulations.

3.6. FTIR analysis of MGF loaded nanoparticles

FTIR spectral analysis of MGF loaded nanoparticles has been depicted through Fig. 3A-C. Absorption bands at 3464 cm^{-1} (Fig. 3A) of NSC and at 3368 cm^{-1} in MGF (Fig. 3B) which is a characteristic band of —OH stretch has been slightly shifted to 3437 cm^{-1} (Fig. 3C) in the

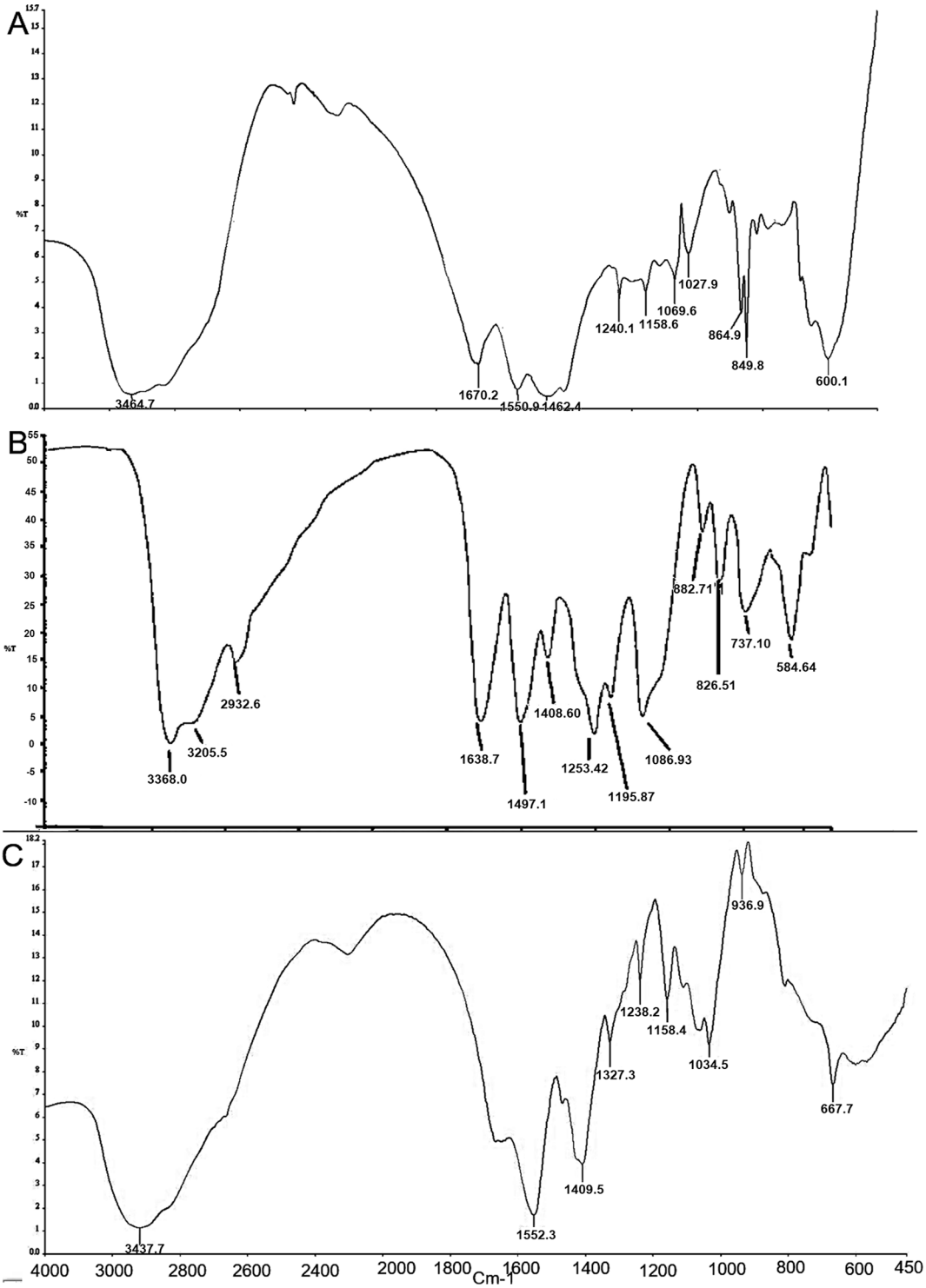

Fig 3. FT-IR spectra of A. *N*-Succinyl chitosan –alginate nanoparticles (blank) B. Pure MGF C. MGF loaded Succinyl chitosan-alginate formulation.

formulation. This mild shifting suggests a possible interaction between corresponding —OH groups of polymer and drug either between themselves or between the —OH and the hydrocarbon backbone of the other. The peak at 1552 cm^{-1} has been picked in Fig. 1C which corresponds to blank NSC-alginate nanoparticle peak at 1551 cm^{-1}. The peaks at 1638 cm^{-1} and 1497 cm^{-1} of pure MGF are revealed to be suppressed in the loaded nanoparticle peak. This suggests that the MGF has been encaged in the nanoparticle formed. In addition to this, a significant number of peaks of MGF from 600 to 950 cm^{-1} has been suppressed in the formulation while formulation peaks in between 950 and 1200 cm^{-1} (Fig. 3C) exhibit shifts compared to both solitary MGF (Fig. 3B) and grafted polymer (Fig. 3A). Hence, successful encapsulation of MGF can be suggested from these spectroscopic characterizations.

3.7. COSY analysis

The $_1H^1$ NMR spectra of NSC has already been demonstrated in section 3.2.

The $_1H^1$ NMR of MGF obtained was as follows:

MGF $_1H^1$ NMR (300 MHz, DMSO-d_6, ppm); δ 3.52 (1H, m, —CH of glycosidic pyranose), δ 3.65 (2H, d, —CH_2 of hydroxyethyl side chain of pyranose), δ 4.08 (1H, t, —OH of —CH_2OH), δ 4.41–4.62 (1H, d, —OH of pyranose), δ 6.13–6.28 (1H, s, phenolic —OH), δ 9.25–9.39 (1H, s, phenolic —OH adjacent to —C═O of pyranose), δ 12.03 (1H, s, phenolic —OH adjacent to —C═O— of pyranose).

From COSY analysis it can be seen that the MGF and NSC interact at several neighbouring protons (Fig. 2). For example, the phenolic —OH of MGF (δ 9.25) interacts with —COOH proton of succinyl side chain (δ 12.38). The same —COOH proton of NSC is observed to react with —CH of glycosidic linkage of MGF (δ 4.95) which connects the pyranose ring to the core of the structure. Again, the —OH proton of MGF of the glycosidic linkage (δ 4.62) is nearer to —NH of succinyl side chain of NSC (δ 8.01) which can be revealed by deep interaction of them in the interaction contour. The aromatic protons of MGF (δ 6.13 ~ 6.28) are also seen to couple with –OH (δ 5.07 ~ 5.47) protons of the–CH_2OH side chain of NSC monomers.

3.8. Particle size estimation of the formulation

The dynamic light scattering (DLS) method was used to estimate the particle size of the nanoparticles. Fig. S4A depicts the particle size distribution of the nanoparticles. The average particle size of the nanoparticles was observed to be 124 nm. The nanoparticles have shown a polydispersity index of 0.322 depicting unimodal particle size distribution and homogeneous distribution of the particles within the suspension. The particle size was further confirmed by scanning electron microscopy (SEM, Hitachi VP SEM, 3400N, Tokyo, Japan). In Fig. S4B, the particle size distribution is suggested to be from 100 to 200 nm although some bigger particle size suggests aggregation. The particle appeared as spherical with a few cornered edges, having a rough surface topography. The size distribution data indicates that the majority of the nanoparticles possess smaller particle size and hence proves its potential in determining oral delivery and action of MGF through the application of the formulation.

3.9. Zeta potential of nanoparticles

In addition to particle size distribution, estimation of zeta potential also plays an integral role in determining effective drug delivery. It helps in interpreting the electrostatic potential of nanoparticle surfaces and subsequently indicates the degree of stability. The zeta potential of the nanoparticles was observed to be – 30 mV as shown in Fig. S5. Negative charges present on the outer surface of succinyl chitosan nanoparticles attributes (one factor may be the ionizable —COOH group present on the grafted polymer surface) to the negative zeta potential of the nanoparticles and hence also offer stability, prevent from self-accumulation and also augments to sustained release of the phytoconstituents. Also, the polydispersity index (PDI) was found as 0.322 suggesting unimodal distribution of the nanoparticle.

3.10. X-ray diffraction

The XRD diffractogram shows substantial peak shifts or peak height appreciation or depreciation in the Formulation (Table S1). For example, MGF peak (2θ = 8.5002) is totally absent in the Formulation. In addition, NSC peak (2θ = 4.8103) has been shifted significantly in the nano-conjugate (2θ = 6.2513). The change of crystallinity is again depicted by the peak heights 550.12 (NSC) & 613.58 (MGF) to Formulation (253.34 and 194.73). Interestingly, absence of several peaks of MGF at 2θ (14.369, 18.915, 10.127) and creation of newer peaks of the formulation at 2θ (12.4304, 12.3084 and 12.8502) suggests several conformational changes, dissociation and association during nano-conjugate formulation. Not only that but the table also indicates that the peak widths have been changed or newer widths have been constructed during formulation which are entirely separated from individual NSC and MGF. This further suggests change in the crystal diameter, shape and size of the formulation than the mother drug (MGF) or the polymer (NSC).

3.11. In vitro drug release study

The *in vitro* release of drug from the polymer matrix showed sigmoidal pattern while tested in PBS pH 7.4 (Intestinal pH, simulating oral administration of NCS-MGF nanoconjugate in diseased condition). Maintaining sink condition, initially the drug (MGF) showed relatively impeded release; where nearly 80% of the drug was seen released within 70 mins (Fig. S6). However, the aftermath of release showed relatively slow pattern where remaining 20% of the drug exhibited release in another 40 mins. Altogether the entire drug encapsulated within the matrix released with 100–120 mins providing no “payload loss” within the reservoir. In contrast, when solitary MGF is allowed to release within same pH under sink condition with temperature and stirring (Fig. S6), around 23.03% of the drug was released within 60 mins which slowed down afterwards and reached plateau phase within 180–240 mins with only 30.25% release (cumulative, w/w).

The release data points were subsequently fitted on various order independent kinetics model with KinetDS and observed that the release fits maximally with Baker-Lonsdale model ($r^2 = 0.9344$, Table S2). This suggest the MGF loaded *N*-succinylated chitosan nanoparticle to be spherical in nature and the drug release is supposed to be from spherical matrix. This is in compliance with the SEM image of the nanoconjugate which also showed near spherical geometry of the NSC-MGF hybrid particle. Interestingly, the model also elicited reasonable fitting with Weibull ($r^2 = 0.9397$) with exponential shape factor 1.15. This finding is in corroboration with the Baker-Lonsdale model since both model suggests the drug-dispersive system as matrix instead of reservoir. However, the shape factor being > 1 suggests initial burst of drug for some time (herein 70–80 mins), then getting sigmoidal afterwards (herein up to 240 mins) (Salome, Godswill, & Ikechukwu, 2013). The detailed kinetic data of model dependent release of NSC-MGF conjugate has been provided in Supplementary data S1.

In order to check Fickian and Non-Fickian release from the Matrix, utilized Korsmeyer-Peppas model fitting ($Mt/M\alpha = K.t^n$)of the drug release kinetics from NSC matrix (supplementary data SD1). The n value was found to be 0.6706 which is considerably above the Fickian diffusion boundary value of 0.43 for spherical matrix. This indicates non-Fickian diffusion probably due to carbohydrate swelling in water, anomalous diffusion of drug from the matrix and presumably an additional erosion factor of the matrix in water.

The Mean Dissolution Time (MDT) and Dissolution efficiency (DE) were calculated as 52.05 mins and 77.52%. However, when solitary MGF was analyzed, MDT and DE were found as 38.23 mins 25.41%. The

clear improvement (3x) of DE of NCS-MGF nano than solitary MGF indicates enhanced dissolution of drug from NCS-MGF conjugate compared to the latter. The MDT enhancement of the former (NCS-MGF) suggests augmented drug retention within the polymeric matrix.

3.12. *In vivo pharmacological activity of drug loaded nanoparticles*

In vivo hypoglycemic responses of MGF loaded nanoparticles were studied by estimation of blood glucose levels and OGTT in different groups of treated animals. FBG levels were determined every seven days, while OGTT was carried out on the 28th day of the study. The diabetic animals were administered with free MGF and nano-formulation of MGF. The dose of MGF in the nanoparticle formulation were similar to that of the free drug i.e. 10 mg/kg dose of MGF was maintained in nanoparticle formulation and free drug treated animal groups.

Blood glucose level in excess of 250 mg/dL were seen with STZ treatment in the DC group. Free MGF (10 mg/kg b.w; MT group) and MGF loaded nanoparticles (10 mg/kg b.w; MNT group) were administered orally for 28 days in the STZ-induced diabetic rats and it was observed that both of them resulted in significant hypoglycemic activity ($p < 0.01$). Interestingly, the hypoglycemic effect of MGF loaded nanoparticles was significantly more pronounced in comparison with that of the free oral MGF ($p < 0.05$), which has been shown in Fig. 4. In the MT group the blood glucose levels reduced by 53.7 % as compared to the DC, whereas, in the MNT group there was a reduction of 73 % in the blood glucose levels on the 28th day of treatment. The group 5, which received only the blank nanoparticles, did not produce any significant reduction in FBG levels ($p > 0.05$), thus ruling out any hypoglycemic activity of the nanocarrier. The significantly higher glycemic control exerted by MGF loaded nanoparticles in STZ induced diabetic rats could be ascribed to the altered release profile of MGF from the nanoparticles. It may very well be assumed that the release of MGF, a weekly basic compound, would have been retarded in stomach, and thereafter in intestinal pH 7.4, the MGF release from the core–shell nanoparticles occurs in a controlled manner, which results in the higher hypoglycemic effectiveness. The results obtained from the *in vitro*MGF release study serves to corroborate this phenomenon.

The efficiency of glucose utilization was evaluated by performing the glucose tolerance test. Poor results obtained with glucose challenge usually indicate towards β cell lysis and/or poor glucose utilization by peripheral tissues. Fig. 5 shows the effect of free MGF and its nanoparticles formulation on blood glucose levels of diabetic animals for duration of 120 mins, where we observed that both the treatments were able to reduce the blood glucose. However, MGF loaded nanoparticles showed more promising reduction in the parameters with 80.3 ± 3.4 mg/dL blood glucose level after 120 mins whereas animal group receiving free MGF showed blood glucose level of 115.93 ± 3.9 mg/dL after 120 mins. The reduction in blood sugar levels for the MT and MNT groups was thus 67.6 % and 77.4 % respectively as compared to the DC ($p < 0.05$).

The oral glucose challenge indicates superior glucose utilization in MGF loaded nanoparticles treated animals as compared to free MGF treated groups ($p < 0.05$). In the group 5, which was treated with blank nanoparticles, there was no reduction in blood glucose levels ($p > 0.05$, compared to the DC group), confirming poor glucose tolerance. The *in vitro* drug release patterns corresponds to that of *in vivo* effects in showing sustained release of drug from the polymer matrix and subsequent glycemic control in diabetic rats.

Serum lipid concentrations in STZ treated rats exhibited very high increase in levels of TGs, total cholesterol and LDL cholesterol as compared to normal control rats. Treatment with MGF and MGF loaded nanoparticles caused 25.5 % and 41.8 % decrease in serum TG concentrations, respectively ($p < 0.05$). Similarly, total cholesterol levels and LDL cholesterol levels were significantly reduced in diabetic rats treated with MGF loaded nanoparticles. Treatment with MGF and MGF loaded nanoparticles caused 20.7 % and 43.39 % decrease in serum TC concentrations ($p < 0.05$), respectively (Table 1). Treatment with MGF and MGF loaded nanoparticles caused 24.4 % and 51.9 % decrease in LDL concentrations, respectively. There was no significant ($p > 0.05$) elevation in the HDLC level in MGF treated diabetic rats on 28th day as compared to the diabetic control group.

MGF is a phytomolecule with pleiotropic effects but the putative clinical benefits are hampered owing to its poor aqueous solubility, low bioavailability, high hepatic first-pass metabolism and high P-glycoprotein efflux (Basheer &Kerem, 2015; Khurana et al., 2017). To overcome the pharmacokinetic handicaps of MGF and explore its therapeutic benefits, encapsulation of MGF in biodegradable polymers appears to be a logical attempt to improve its bioavailability. Since NSC has been evolved as a polymer over the last few years as a biocompatible carrier, the first crucial step of our study has been *N*-succinylation of chitosan which has been successfully achieved as revealed by FT-IR and $_1H^1$ NMR studies. Afterwards, COSY analysis revealed coupling interaction between MGF and NSC especially in between –OH of MGF and —C═O, —NH—, carboxyl of side chain —NHC═OCH_2CH_2COOH in NSC which has been in compliance with our pre-formulation molecular docking studies between the same duo. The release followed Baker-Lonsdale pattern probably due to the near spherical shape of the formulation as revealed in SEM micrograph. The formulation revealed zeta potential

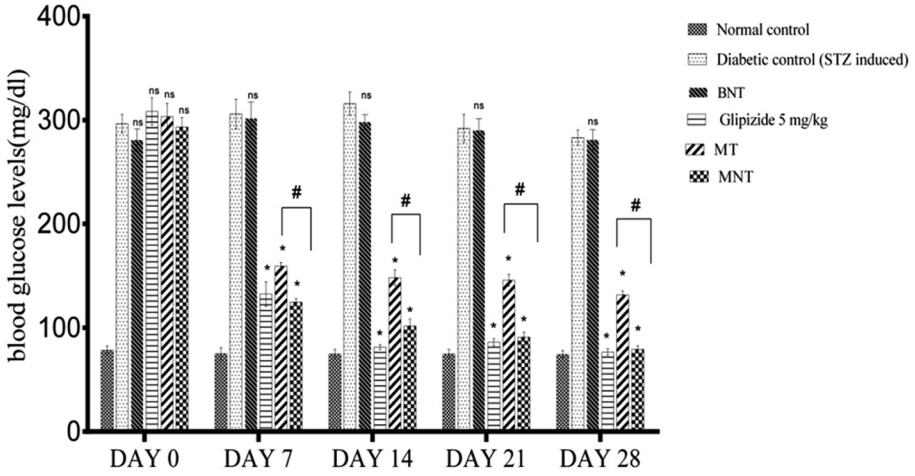

Fig 4. Effect of oral free MGF (MT) and oral MGF loaded core–shell nanoparticles (MNT) on blood glucose levels in diabetic rats. All values are expressed in Mean ± SEM (n = 6) * denotes $p < 0.01$, compared with DC group.# denotes $p < 0.05$, compared amongst MT and MNT group.ns denotes $p > 0.05$, non-significant as compared to the DC group.

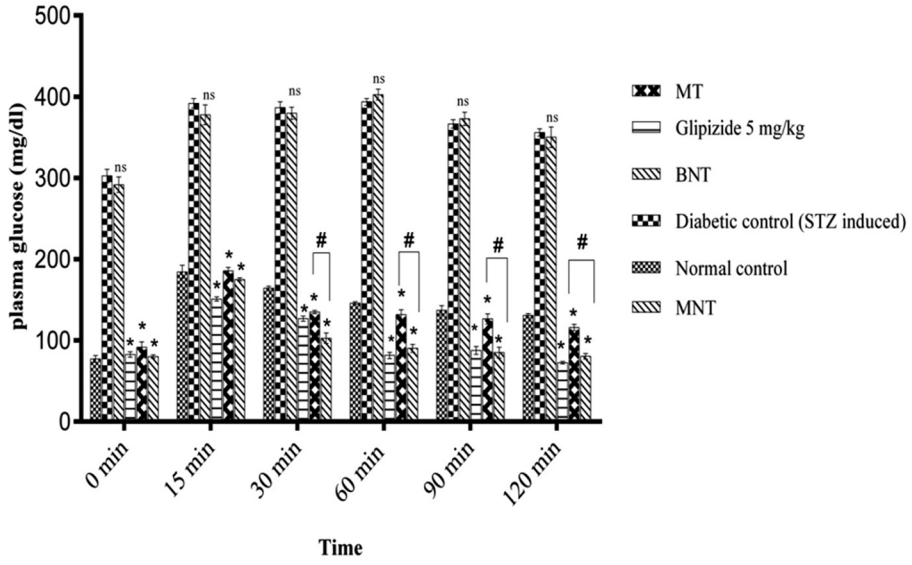

Fig 5. Effect of oral free MGF (MT) and oral MGF loaded core–shell nanoparticles (MNT) on glucose tolerance in diabetic rats. All values are expressed in Mean ± SEM (n = 6) * denotes $p < 0.05$, compared with DC group. # denotes $p < 0.05$, compared amongst MT and MNT group. ns denotes $p > 0.05$, non-significant as compared to the DC group.

Table 1
Effect of oral Free MGF (MT) and oral MGF loaded core–shell nanoparticles (MNT) on serum lipid profile in diabetic rats.

Lipid profile	Days	Normal control	Diabetic control	Glipizide 5 mg/kg	Diabetic + MT	Diabetic + MNT
TC	Day 0	115.3 ± 3.2	187.6 ± 2.6	185.2± 4.6	190.5± 4.9	194.3 ± 5.8
	Day 28	121 ± 4.6	237 ± 5.3	118.6±2.6*	145.2±3.2*	122.3 ± 1.9 *#
TG	Day 0	83.6 ± 2.5	142.6 ± 4.1	140.8± 2.1	151.8± 5.1	154.2 ± 4.6
	Day 28	86.8 ± 3.8	166.1 ± 5.2	87.3 ± 1.2 *	115.3±3.3*	84.9± 1.3 *#
LDL C	Day 0	48.2 ± 1.2	128 ± 6.3	125 ± 5.6	139.7± 2.6	142.5 ± 4.2
	Day 28	50.6 ± 2.4	172.3 ± 4.5	51.3±2.2*	79.2±0.8*	55.4 ± 3.3 *#
HDL C	Day 0	51.6 ± 3.2	42.3 ± 1.7	41.6± 0.9	42.9± 1.6	41.8± 1.8
	Day 28	52.8 ± 2.9	33.8 ± 2.6	52.4±1.5*	44.3±3.2*	49.6±2.2*

All values are expressed in Mean ± SEM (n = 6)
* denotes $p < 0.05$ compared with diabetic control group.
# denotes $p < 0.05$ compared amongst MT and MNT group.
Abbreviations: TC, total cholesterol; TG, triglycerides; LDL C, low density lipoprotein cholesterol; HDL C, high density lipoprotein cholesterol; BNT, blank nanoparticles; MT, free MGF treated; MNT; MGF nanoparticle treated

suggesting its stability probably due to the ionizable —COOH groups over the surface of the polymer. We assume that the abundant negatively charged —COOH terminals may help to create the stable electric double layer ultimately leading to stable zeta potential. The XRD diffractogram also exhibited change of crystallinity of the nano-conjugate showing size, shape and diameter of the crystal.

Diabetic rats were orally administered with 10 mg/kg b.w. MGF loaded nanoparticles (MNT group) and free MGF (MT group) for a period of 28 days and blood glucose levels were estimated every 7 days. On completion of the 28 days of treatment in the group 6 (MNT), the diabetic rats were found to almost normoglycemic (FBG levels of 81.5 ± 3.3 mg/dL), whereas group 4 (MT) continued to be hyperglycemic (FBG levels of 128.3 ± 2.8 mg/dL) as compared to MNT group ($p < 0.01$). This improved glycemic control could be due to protective activity of MGF on β-cells as pointed out by (Sellamuthu et al., 2013), where the protective effects of MGF on pancreatic β-cells in STZ induced diabetic rats MGF has been established (Sellamuthu et al., 2013). Furthermore, MGF has been found to improve insulin sensitivity and alleviate genetic or environment induced IR. Improved glucose utilization by MGF has been attributed to increased GLUT 4 activity and improved glycogenesis (Girón et al., 2009; Sellamuthu et al., 2013; Zhang et al., 2019). Simultaneously the improved response to glucose challenge by the rats of group 6 (MNT) confirms significant improvement in glucose utilization, indicating improved glucose homeostasis. The improved therapeutic efficiency of oral MGF-encapsulated nanoparticles could be attributed to the controlled release of MGF from the polymeric nanoparticles.

The role of dyslipidemia in the development of diabetic macrovasular complications has been long known, atherosclerosis being a major pathological development which ultimately culminates into cardio vascular emergencies (Defronzo, 2009). Impaired glucose utilization (possibly due to IR) and increased hepatic glucose output by gluconeogenesis has been associated with increased lipolysis, which leads to elevated serum lipid levels. Serum triglyceride and cholesterol levels were significantly higher in STZ induced diabetic rats, as shown in Table 1. Treatment with encapsulated nano-conjuagated MGF significantly lowered triglycerides and cholesterol levels by day 28 ($p < 0.05$). It has been observed that treating diabetes induced hyperlipidemia with solitary MGF reduced plasma cholesterol either ~ 1% (Dineshkumar, Mitra, & Manjunatha, 2010) or reduced 14% (Gururaja et al., 2017), 25% (Miura et al., 2001), 36.84% (Muruganandan et al., 2005) in 10–30 mg/kg for 28–30 days in rodent models. On the contrary our NSC-MGF nano-formulation reduced plasma cholesterol 37.13% at only 10 mg/kg for 28 days. Not only total plasma cholesterol, but also total triglycerides reduced ~ 61 % by our NSC-MGF treatment whereas in the reported works the triglycerides reduced maximally from 10 ~ 40%. Thus, the

NSC-MGF hypolipidemic activity is comparable or better than the earlier citations with solitary MGF. Not only this, but the NSC-MGF output was also found to be comparable or marginally better than that of standard glipizide. Lowering of total cholesterol and LDL cholesterol levels demonstrates the anti-atherosclerotic potential of NSC-MGF loaded nanoparticles in diabetic conditions. It was observed that there was no significant increase in levels of HDL cholesterol in the MT and MNT treated groups.

4. Conclusion

In our quest of achieving successful oral delivery of MGF, we have incorporated MGF in a structured nano-assembly system comprising of NSC and alginate. The nanoparticles were characterized by FT-IR, XRD, $_1H^1$ NMR, COSY, DLS and SEM. The MGF loaded nanoparticles showed comprehensive MGF encapsulation efficiency of 88%. The nano-formulation was able to produce better controlled release of MGF following non-fickian diffusion mechanism. The MGF loaded nanoparticles produced significant hypoglycemic response and hypolipidemic responses following oral delivery in diabetic rats which is comparable or better to the earlier reports in this field. The results suggest the successful preparation of NSC-MGF nanoconjugate which may be a promising nanomedicine for management of hyperglycemia and asssociated hyperlipidemia in future.

Declaration of Competing Interest

The authors declare that they have no known competing financial interests or personal relationships that could have appeared to influence the work reported in this paper.

Acknowledgements

The authors are highly thankful to Innoscience Research Sdn. Bhd, Malaysia for financial support in this work. Also, the authors are also thankful to Dr. B.C. Roy College of Pharmacy & Allied Health Sciences, Durgapur, WB, India for providing the necessary infrastructure for this work.

Appendix A. Supplementary data

Supplementary data to this article can be found online at https://doi.org/10.1016/j.foodchem.2021.131376.

References

Alam, S., Hasan, M. K., Neaz, S., Hussain, N., Hossain, M. F., & Rahman, T. (2021). Diabetes mellitus: Insights from epidemiology, biochemistry, risk factors, diagnosis. *Complications and Comprehensive Management. Diabetology, 2*(2), 36–50. https://doi.org/10.3390/diabetology2020004

Aswal, S., Kumar, A., Chauhan, A., Semwal, R. B., Kumar, A., & Semwal, D. K. (2020). A molecular approach on the protective effects of mangiferin against diabetes and diabetes-related complications. *Current Diabetes Review, 16*(7), 690–698. https://doi.org/10.2174/1573399815666191004112023

Basheer, L., & Kerem, Z. (2015). Interactions between CYP3A4 and Dietary Polyphenols. *Oxidative Medicine and Cellular Longevity, 2015*, 1–15. https://doi.org/10.1155/2015/854015

Bashir, S., Teo, Y. Y., Ramesh, S., Ramesh, K., & Khan, A. A. (2015). N-succinyl chitosan preparation, characterization, properties and biomedical applications: A state of the art review. In Reviews in Chemical Engineering (Vol. 31, Issue 6, pp. 563–597). Walter de Gruyter GmbH. doi:10.1515/revce-2015-0016.

Choi, J. H., Banks, A. S., Estall, J. L., Kajimura, S., Boström, P., Laznik, D., … Spiegelman, B. M. (2010). Anti-diabetic drugs inhibit obesity-linked phosphorylation of PPARγ 3 by Cdk5. *Nature, 466*(7305), 451–456. https://doi.org/10.1038/nature09291

de Souza, J. R. R., Feitosa, J. P. A., Ricardo, N. M. P. S., Trevisan, M. T. S., de Paula, H. C. B., Ulrich, C. M., & Owen, R. W. (2013). Spray-drying encapsulation of mangiferin using natural polymers. *Food Hydrocolloids, 33*(1), 10–18. https://doi.org/10.1016/j.foodhyd.2013.02.017

Defronzo, R. A. (2009). From the triumvirate to the ominous octet: A new paradigm for the treatment of type 2 diabetes mellitus. *Diabetes, 58*(4), 773–795. https://doi.org/10.2337/db09-9028

Di Pino, A., & Defronzo, R. A. (2019). Insulin resistance and atherosclerosis: Implications for insulin-sensitizing agents. *Endocrine Reviews, 40*(6), 1447–1467. https://doi.org/10.1210/er.2018-00141

Dineshkumar, B., Mitra, A., & Manjunatha, M. (2010). Studies on the anti-diabetic and hypolipidemic potentials of mangiferin (xanthone glucoside) in streptozotocin-induced type 1 and type 2 diabetic model rats. *International Journal of Advances in Pharmaceutical Sciences, 1*(1), 75–85. https://doi.org/10.5138/ijaps.2010.0976.1055.01009

Du, S., Liu, H., Lei, T., Xie, X., Wang, H., He, X., …, & Wang, Y. (2018). Mangiferin: An effective therapeutic agent against several disorders (Review). In Molecular Medicine Reports (Vol. 18, Issue 6, pp. 4775–4786). Spandidos Publications. doi:10.3892/mmr.2018.9529.

Ferreira, F.d. R., Valentim, I. B., Ramones, E. L. C., Trevisan, M. T. S., Olea-Azar, C., Perez-Cruz, F., … Goulart, M. O. F. (2013). Antioxidant activity of the mangiferin inclusion complex with β-cyclodextrin. *LWT - Food Science and Technology, 51*(1), 129–134. https://doi.org/10.1016/j.lwt.2012.09.032

Gaikwad, S. B., Krishna Mohan, G., & Rani, M. S. (2014). Phytochemicals for diabetes management. *Pharmaceutical Crops, 5*(1), 11–28.

Girón, M. D., Sevillano, N., Salto, R., Haidour, A., Manzano, M., Jiménez, M. L., … López-Pedrosa, J. M. (2009). Salacia oblonga extract increases glucose transporter 4-mediated glucose uptake in L6 rat myotubes: Role of mangiferin. *Clinical Nutrition, 28*(5), 565–574. https://doi.org/10.1016/j.clnu.2009.04.018

Gupta, R. (2018). Active phytoconstituents for diabetes management: A review. In Journal of Complementary and Integrative Medicine (Vol. 15, Issue 3). De Gruyter. doi:10.1515/jcim-2017-0123.

Gururaja, G. M., Mundkinajeddu, D., Senthil Kumar, A., Dethe, S. M., Joshua Allan, J., & Agarwal, A. (2017). Evaluation of cholesterol-lowering activity of standardized extract of Mangifera indica in albino Wistar rats. *Pharmacognosy Research, 9*(1), 21–26. https://doi.org/10.4103/0974-8490.199770

Hossain, M. A., Alam, S., & Paul, P. (2013). Development and evaluation of sustained release matrix tablets of Indapamide using methocel K15M CR. *Journal of Applied Pharmaceutical Science, 3*(5), 85–90. https://doi.org/10.7324/JAPS.2013.3516

Hou, J., Zheng, D., Fung, G., Deng, H., Chen, L., Liang, J., … Hu, Y. (2013). Mangiferin mitigates diabetic cardiomyopathy in streptozotocin-diabetic rats. In J. Physiol. Pharmacol. Downloaded from www.nrcresearchpress.com by. www.nrcresearchpress.com.

Kamoun, E. A. (2016). N-succinyl chitosan-dialdehyde starch hybrid hydrogels for biomedical applications. *Journal of Advanced Research, 7*(1), 69–77. https://doi.org/10.1016/j.jare.2015.02.002

Katakami, N. (2018). Mechanism of development of atherosclerosis and cardiovascular disease in diabetes mellitus. *Journal of Atherosclerosis and Thrombosis, 25*(1), 27–39. https://doi.org/10.5551/jat.RV17014

Kato, Y., Onishi, H., & Machida, Y. (2004). N-succinyl-chitosan as a drug carrier: Water-insoluble and water-soluble conjugates. In Biomaterials (Vol. 25, Issue 5, pp. 907–915). Elsevier BV. doi:10.1016/S0142-9612(03)00598-2.

Kaur, P., Kumar, M., Parkash, J., & Prasad, D. N. (2019). Oral hypoglycemic drugs: An overview. Journal of Drug Delivery and Therapeutics, 9(s), 770–777. doi:10.22270/jddt.v9i3-s.2815.

Khurana, R. K., Bansal, A. K., Beg, S., Burrow, A. J., Katare, O. P., Singh, K. K., & Singh, B. (2017). Enhancing biopharmaceutical attributes of phospholipid complex-loaded nanostructured lipidic carriers of mangiferin: Systematic development, characterization and evaluation. *International Journal of Pharmaceutics, 518*(1–2), 289–306. https://doi.org/10.1016/j.ijpharm.2016.12.044

la Sala, L., Prattichizzo, F., &Ceriello, A. (2019). The link between diabetes and atherosclerosis. European Journal of Preventive Cardiology, 26(2_suppl), 15–24. doi:10.1177/2047487319878373.

Luna, B., & Feinglos, M. (2001). Oral Agents in the Management of Type 2 Diabetes Mellitus. *American Family Physician, 63*(9), 1747–1756.

Ma, H., Chen, H., Sun, L., Tong, L., & Zhang, T. (2014). Improving permeability and oral absorption of mangiferin by phospholipid complexation. *Fitoterapia, 93*, 54–61. https://doi.org/10.1016/j.fitote.2013.10.016

May, M., & Schindler, C. (2016). Clinically and pharmacologically relevant interactions of antidiabetic drugs. In Therapeutic Advances in Endocrinology and Metabolism (Vol. 7, Issue 2, pp. 69–83). SAGE Publications Ltd. doi:10.1177/2042018816638050.

Miura, T., Iwamoto, N., Kato, M., Ichiki, H., Kubo, M., Komatsu, Y., … Tanigawa, K. (2001). Effect of mangiferin on muscle GLUT4 protein content in TSOD (Tsumura, Suzuki, Obese, Diabetes) mouse, a new type 2 diabetic mice. Biomedical Research, 22(5), 249–252. doi:10.2220/biomedres.22.249.

Mukhopadhyay, P., Maity, S., Chakraborty, S., Rudra, R., Ghodadara, H., Solanki, M., … Kundu, P. P. (2016). Oral delivery of quercetin to diabetic animals using novel pH responsive carboxypropionylated chitosan/alginate microparticles. RSC Advances, 6(77), 73210–73221. doi:10.1039/c6ra12491g.

Mukhopadhyay, P., Maity, S., Mandal, S., Chakraborti, A. S., Prajapati, A. K., & Kundu, P. P. (2018). Preparation, characterization and in vivo evaluation of pH sensitive, safe quercetin-succinylated chitosan-alginate core-shell-corona nanoparticle for diabetes treatment. *Carbohydrate Polymers, 182*, 42–51. https://doi.org/10.1016/j.carbpol.2017.10.098

Mukhopadhyay, P., Sarkar, K., Bhattacharya, S., Bhattacharyya, A., Mishra, R., & Kundu, P. P. (2014). PH sensitive N-succinyl chitosan grafted polyacrylamide hydrogel for oral insulin delivery. *Carbohydrate Polymers, 112*, 627–637. https://doi.org/10.1016/j.carbpol.2014.06.045

Muruganandan, S., Srinivasan, K., Gupta, S., Gupta, P. K., & Lal, J. (2005). Effect of mangiferin on hyperglycemia and atherogenicity in streptozotocin diabetic rats. *Journal of Ethnopharmacology, 97*(3), 497–501. https://doi.org/10.1016/j.jep.2004.12.010

Ohiagu, F. O., Chikezie, P. C., & Chikezie, C. M. (2021). Pathophysiology of diabetes mellitus complications: Metabolic events and control. *Biomedical Research and Therapy, 8*(3), 4243–4257. https://doi.org/10.15419/bmrat.v8i3.663

Pal, Pabitra Bikash, Sinha, Krishnendu, Sil, Parames C., & Srinivasula, Srinivasa M. (2014). Mangiferin attenuates diabetic nephropathy by inhibiting oxidative stress mediated signaling cascade, TNFα related and mitochondrial dependent apoptotic pathways in streptozotocin-induced diabetic rats. *PLoS ONE, 9*(9), e107220. https://doi.org/10.1371/journal.pone.0107220

Papatheodorou, K., Banach, M., Bekiari, E., Rizzo, M., & Edmonds, M. (2018). Complications of Diabetes 2017. In Journal of Diabetes Research (Vol. 2018). Hindawi Limited. doi:10.1155/2018/3086167.

Poznyak, Anastasia, Grechko, Andrey V., Poggio, Paolo, Myasoedova, Veronika A., Alfieri, Valentina, & Orekhov, Alexander N. (2020). The diabetes mellitus–atherosclerosis connection: The role of lipid and glucose metabolism and chronic inflammation. *International Journal of Molecular Sciences, 21*(5), 1835. https://doi.org/10.3390/ijms21051835

Saleh, S., El-Maraghy, N., Reda, E., & Barakat, W. (2014). Modulation of diabetes and dyslipidemia in diabetic insulin-resistant rats by mangiferin: Role of adiponectin and TNF-α. *Anais Da Academia Brasileira de Ciencias, 86*(4), 1935–1947. https://doi.org/10.1590/0001-3765201420140212

Salome, A. C., Godswill, C. O., & Ikechukwu, I. O. (2013). Kinetics and mechanisms of drug release from swellable and non swellable matrices: A review. *Research Journal of Pharmaceutical, Biological and Chemical Sciences, 4*(2), 97–103.

Sellamuthu, P. S., Arulselvan, P., Muniappan, B. P., Fakurazi, S., & Kandasamy, M. (2013). Mangiferin from salacia chinensis prevents oxidative stress and protects pancreatic β-cells in streptozotocin-induced diabetic rats. *Journal of Medicinal Food, 16*(8), 719–727. https://doi.org/10.1089/jmf.2012.2480

Sellamuthu, P. S., Muniappan, B. P., Perumal, S. M., & Kandasamy, M. (2009). Antihyperglycemic effect of mangiferin in streptozotocin induced diabetic rats. *Journal of Health Science, 55*(2), 206–214. https://doi.org/10.1248/jhs.55.206

Silva, E. F. F., Ferreira, C. M. M., & de Pinho, L. (2017). Risk factors and complications in type 2 diabetes outpatients. *Revista Da Associacao Medica Brasileira, 63*(7), 621–627. https://doi.org/10.1590/1806-9282.63.07.621

Simionato, L. D., Petrone, L., Baldut, M., Bonafede, S. L., & Segall, A. I. (2018). Comparison between the dissolution profiles of nine meloxicam tablet brands commercially available in Buenos Aires, Argentina. *Saudi Pharmaceutical Journal, 26*(4), 578–584. https://doi.org/10.1016/j.jsps.2018.01.015

Singh, R., Kaur, N., Kishore, L., & Kumar Gupta, G. (2013). Management of diabetic complications: A chemical constituents based approach. *Journal of Ethnopharmacology, 150*(1), 51–70. https://doi.org/10.1016/j.jep.2013.08.051

Stein, S. A., Lamos, E. M., & Davis, S. N. (2013). A review of the efficacy and safety of oral antidiabetic drugs. *Expert Opinion on Drug Safety, 12*(2), 153–175. https://doi.org/10.1517/14740338.2013.752813

Stolar, Mark W., & Chilton, Robert J. (2003). Type 2 diabetes, cardiovascular risk, and the link to insulin resistance. *Clinical Therapeutics, 25*, B4–B31. https://doi.org/10.1016/S0149-2918(03)80240-0

Tsang, M.-W. (2012). The Management of Type 2 Diabetic Patients with Hypoglycaemic Agents. *ISRN Endocrinology, 2012*, 1–9. https://doi.org/10.5402/2012/478120

Yan, C., Chen, D., Gu, J., Hu, H., Zhao, X., &Qiao, M. (2006). Preparation of N-Succinyl-chitosan and Their Physical-Chemical Properties as a Novel Excipient.

Yang, Xuemin, Zhao, Yulin, Chen, Yunjian, Liao, Xiali, Gao, Chuanzhu, Xiao, Dan, … Yang, Bo (2013). Host-guest inclusion system of mangiferin with β-cyclodextrin and its derivatives. *Materials Science and Engineering C, 33*(4), 2386–2391. https://doi.org/10.1016/j.msec.2013.02.002

Zhang, Qiao, Kong, Xiangju, Yuan, Hang, Guan, Hongjun, Li, Ying, & Niu, Yucun (2019). Mangiferin improved palmitate-induced-insulin resistance by promoting free fatty acid metabolism in HepG2 and C2C12 cells via PPARα: Mangiferin improved insulin resistance. *Journal of Diabetes Research, 2019*, 1–13. https://doi.org/10.1155/2019/2052675